

Introduction to XRD analysis of modern functional thin films using a 2-dimensional detector— (1) GI-XRD

Shintaro Kobayashi* and Katsuhiko Inaba**

1. Introduction

The development of new functional thin films and the fabrication of functional devices using these materials are the outgrowth of emerging demands for high efficiency, energy-saving, lightweight devices to further the pursuit of comfort and convenience in daily life. The “Smartphone” is a typical example, where numerous functional thin film based devices are employed, such as, display screens, backlighting, batteries, data storage devices, etc. Characterization of functional thin films is necessary in terms of not only the phase identification of composing materials but also further crystallographic characterization of constituent crystals, such as their textures or orientation relationships with substrates, lattice distortions, film thicknesses etc., since these physical parameters are closely correlated with the devices’ performance.

A 2-dimensional (2D) detector enables various kinds of XRD measurements to be performed in a remarkably short time, covering a wide range of reciprocal space^{(1)–(4)} and thus, enables us to perform certain measurements with laboratory equipment that have previously been performed only at synchrotron facilities. Recently, the hybrid pixel array 2-dimensional detector (HPAD) has come into use for measurements with in-house XRD systems. The Rigaku SmartLab™ X-ray diffractometer can also be equipped with the latest HPAD, the “HyPix-3000”.⁽²⁾ This detector is equipped with direct X-ray detection pixel array sensors, which enable capabilities such as high sensitivity, wide-dynamic range, and high spatial resolution.

Examples of X-ray analysis of modern functional thin film materials using 2D detectors are presented in this short series of articles. The article, Part 1 is focused on examples of polycrystalline thin films specimens, where how to effectively collect weak signals from thin films is crucial for the analysis. The forthcoming Part 2 article will be dedicated to cases featuring the analysis of epitaxial thin films with complex domain structures.

2. Concept of GI-XRD with 2D detector for polycrystalline thin film analysis

A Grazing Incidence (GI) XRD technique, where an incident X-ray beam strikes a specimen surface at a very shallow angle, is often employed for the measurement of ultra-thin film specimens, since their very weak

signals can be effectively observed with this technique. Moreover, a 2D detector is a very powerful tool for the determination of the preferred orientation textures of thin film specimens,^{(1)–(4)} thereby enabling easier measurement by employing a 2D detector in GI-XRD measurements. In using a 2D detector however, the point-shaped beam is invariably required for the incident X-rays. Furthermore, a grazing incidence geometry requires a very narrow beam to avoid over-footprints. The diameter of the incident X-ray beam in GI-XRD with 2D detector should therefore be set to less than 0.1 mm.⁽⁵⁾

Figure 1 shows a schematic illustration of a typical example of geometry for GI-XRD with a 2D detector. In general, an incident X-ray beam is shaped like a point by using a pin-hole collimator. The angle of the incident X-rays is usually set around a critical angle for the total external reflection of the film (or surface) layer. In case of organic film, this angle is set to 0.15–0.20° with X-rays of Cu $K\alpha$ radiation.⁽⁶⁾ The incident X-rays will be diffracted at the film layer and the diffracted X-rays will spread out like a “cone.” A 2D detector placed downstream below the specimen records a part of the Debye–Scherrer ring as a diffraction image. The missing part of the ring is lost mainly due to being shielded by the specimen itself. Since this image contains information from the scattering angle (thus, d value of lattice spacing) and of the geometrical distribution against the surface area of the specimen, it is possible to evaluate the direction and degree of preferred orientation of the film layer. In the figure, the normal direction of the surface of the specimen on a 2D detector is usually denoted as “Stacking direction (Q_z)”

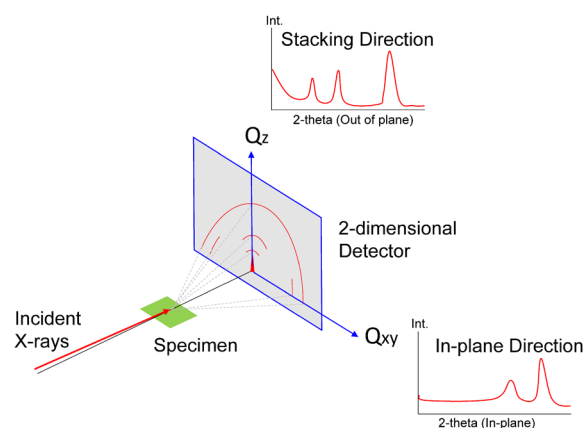


Fig. 1. Geometry of GI-XRD with 2-dimensional detector.

* Application Laboratories, Rigaku Corporation.

** X-ray Research Laboratory, Rigaku Corporation.

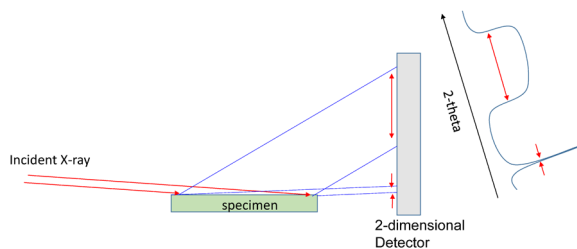


Fig. 2. Projection of sample size in GI-XRD geometry on 2-dimensional detector.

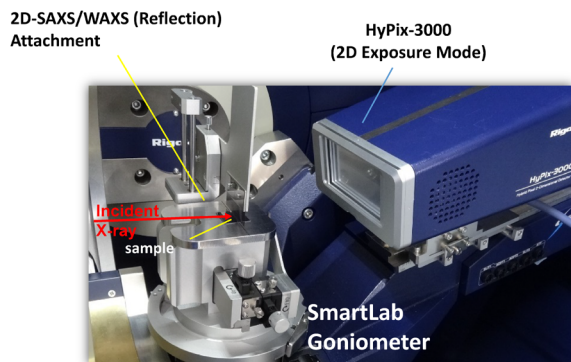


Fig. 3. 2D-SAXS/WAXS (reflection) attachment equipped on SmartLab+HyPix-3000 system.

for easy description, but this is not actually correct. This directional information with this geometry of measurement is the same as “incident angle fixed, 2θ scan”, where the measurement direction (*i.e.*, scattering vector) is tilted to the direction of the incident X-rays. The degree of tilting is calculated as: (*half of 2θ value*) – (*incident angle*). In the case of measuring a specimen with a strong preferred orientation texture for stacking direction, signals from reflections of a higher order index will be missed due to the deviation of measurement direction during analysis.

The range of the scattering angle covered by a 2D detector at a fixed position of 2θ can be controlled by changing the distance from the center of the goniometer (or specimen) to the detector. If there is a short distance between the center of the goniometer and detector, the observable range of the scattering angle will be wider due to the increased capture angle of the detector window. This wide range measurement with GI geometry is called, “GI-Wide Angle X-ray Scattering” (GI-WAXS). Conversely, the measurement dedicated especially to the range of small scattering angles with a long distance from the center of the goniometer to detector, where higher spatial resolution is realized, is called, “GI-Small Angle X-ray Scattering” (GI-SAXS). Note that both techniques use grazing incidence X-rays, so that the width of diffracted beam will be wider in the case of high a 2θ angle (Fig. 2).

Figure 3 shows a picture of the latest 2D-SAXS/WAXS (Reflection) attachment equipped on the SmartLab+HyPix-3000 system, and Fig. 4 shows the detail of this attachment. By installing this attachment on

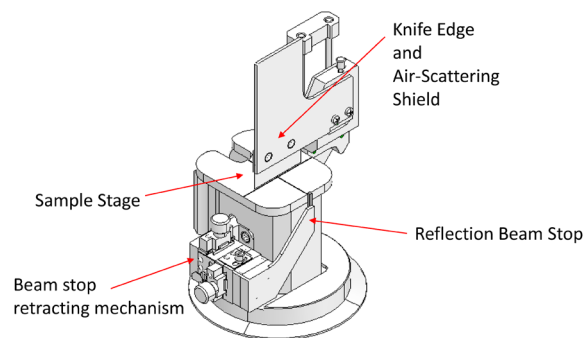


Fig. 4. The detail of 2D-SAXS/WAXS (reflection) attachment.

a SmartLab+HyPix-3000 system, a clear 2-dimensional diffraction image can be obtained.

For this analysis, a specimen is set on the center of a stage. A knife edge and scattering shield are placed above the specimen to suppress the effect of the air scattering caused by the incident X-ray beam. A position-adjustable beam stop of variable size can also be employed, to cut the direct X-rays and suppress scattering from the specimen’s surface, in order to achieve superior contrast from the weak diffraction of the thin film layer.

In next section, some experimental results for polycrystalline specimens will be shown as an introduction to GI-XRD. All 2-dimensional data were measured by a Rigaku SmartLab+HyPix-3000 system equipped with a 2D-SAXS/WAXS (reflection) attachment.

3. Analytical examples of polycrystalline thin films

3.1. Texture analysis of ultra-thin AZO film

ZnO thin film is widely used in the fields of solar cells, displays, and more recently as transparent conductive oxide (TCO) electrodes. The structure of ZnO crystal is known as a wurtzite-type structure with hexagonal symmetry and deposited films mostly exhibit a [0001] (*c*-axis) crystallographic preferred orientation texture along a stacking direction.⁽⁷⁾⁻⁽⁹⁾ This orientation information can be found from strong peaks of 000/ l ($l=2n$; n =integer) reflections by performing the $\theta/2\theta$ measurement when the film thickness is larger. This orientation texture is expected to be formed at the initial stage of film growth.⁽¹⁰⁾ In case of ultra-thin film, however, it is difficult to obtain diffracted signals of adequate intensity from film layers by performing the $\theta/2\theta$ scan. This situation is caused by the fact that an incident angle is increasing during the $\theta/2\theta$ scan, and thus, the path of incident X-rays in a layer is getting too short to produce sufficient signals from an ultra-thin layer. GI-XRD can be a powerful tool for a measurement of ultra-thin films.

Figure 5 shows a 2-dimensional diffraction image of ultra-thin Al doped ZnO (AZO) film deposited on glass substrate. The incident angle of incoming X-rays was set to 0.35°. The AZO film was deposited by

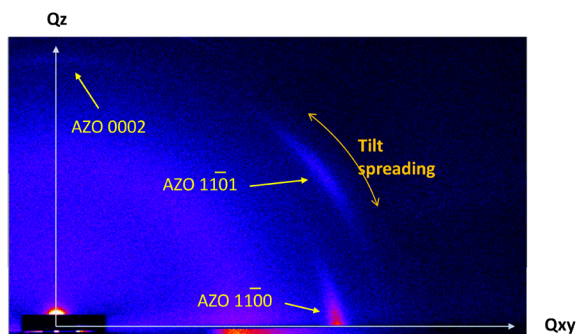


Fig. 5. 2-dimensional diffraction image of ultra-thin AZO film on glass substrate.

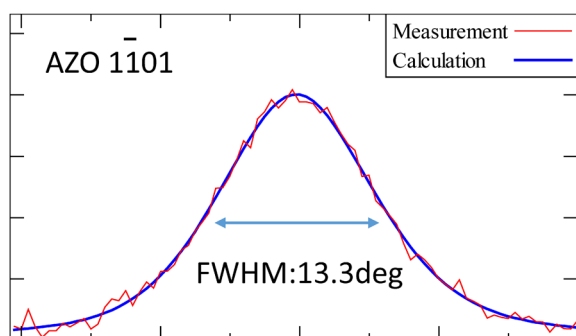


Fig. 6. Tilt spreading profile of AZO $1\bar{1}01$ diffraction.

DC magnetron sputtering^{(10),(11)} and its thickness was determined to be 10.6 nm by X-ray reflectivity analysis. On this figure, some diffraction spots were detected and are identified as AZO 0002, $1\bar{1}01$, $1\bar{1}00$ reflections from their d -values. This result clearly exploits a c -axis preferred orientation texture of AZO film, even though its thickness is extremely thin, around 10 nm, which can be assumed to represent a very early stage of film growth. As explained in Sec. 2, we must be mindful in the analysis of the tilting-effect of the scattering vector. The scattering angle for AZO 0002 reflection with Cu-K α is around 34.4° . Consequently, signals of AZO 0002 reflection on the Q_z axis in Fig. 5 are the ones from crystallites being tilted and deviated by 17.2° ($34.4/2$) from surface's normal direction. Instead of AZO 0002, clear AZO $1\bar{1}01$ reflection was chosen to evaluate the degree of preferred orientation (tilt spreading). The employment of AZO $1\bar{1}01$ reflection for the analysis is favorable in relation to the deviation of the scattering vector above, since its coordinate along Q_z axis is relatively small. The existence of the component along the Q_{xy} direction, however, results in turn in the deviation in the azimuthal (in-plane) direction, which is critical for cases of epitaxial films. As for the present case, AZO film is grown on glass substrate, it is therefore expected that this film is of random orientation texture within the surface plane, so that the deviation effect in the azimuthal direction may be negligible. The peak profile is shown in Fig. 6 and its FWHM value was calculated as 13.3° by a profile fitting.

It should be noted here that a TDI scan^{(1),(2),(4)} with

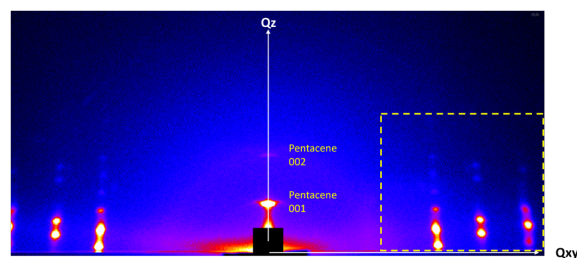


Fig. 7. GI-WAXS image of pentacene thin film on Si substrate.

a 2D detector is a powerful tool for collecting signals along a fixed direction of a scattering vector. The TDI scan with a 2D detector, in a symmetric $\theta/2\theta$ scan mode, can record signals along the Q_z direction as well as the tilting spread along the circumferential direction (almost parallel to Q_{xy} direction), simultaneously. The TDI scan with 2D detector by a symmetric $\theta/2\theta$ scan mode is therefore well matched to the measurement of a thick specimen with a strong preferred orientation texture. A good example is shown in the Fig. 2 of Ref. (11). Both modes of GI-WAXS/SAXS measurement in snapshot mode and in TDI scan mode are available with SmartLab + HyPix-3000 system.

3.2. Crystal structure analysis of pentacene thin film on Si substrate

Pentacene is a popular organic semiconductor material and is widely studied as a promising candidate for organic thin film transistors (TFT). It is reported that the metastable phase (thin film phase) with a different molecular packing from the bulk stable phase is stabilized in the form of thin films.⁽¹²⁾⁻⁽¹⁴⁾ We have tried to identify the structure of pentacene thin film by comparing it with simulation and experimental diffraction images. Figure 7 shows a diffraction image of pentacene thin film on Si substrate⁽¹⁴⁾ measured by GI-WAXS geometry with the incident angle of 0.12° .

Although the exposure time is as short as 30 min, even with a laboratory XRD system, clear diffraction spots were observed on the 2-dimensional diffraction image. Some spots observed along Q_z axis were indexed as $00l$ reflections of pentacene, revealing a strong (001) preferred orientation texture of the pentacene layer.

Figure 8 (left-up and left-down) shows the result of reciprocal space simulation of a pentacene of thin film phase and of a bulk phase, respectively, with a (001) preferred orientation texture. As can be clearly seen, patterns of reciprocal space map for the thin film phase and the bulk phase are different due to the differences in their structures. Since the experimental image was identical to the simulation pattern of the thin film phase, this specimen was determined to be pentacene of a thin film phase with a (001) preferred orientation texture, and all of observed spots could be indexed along with this determination.

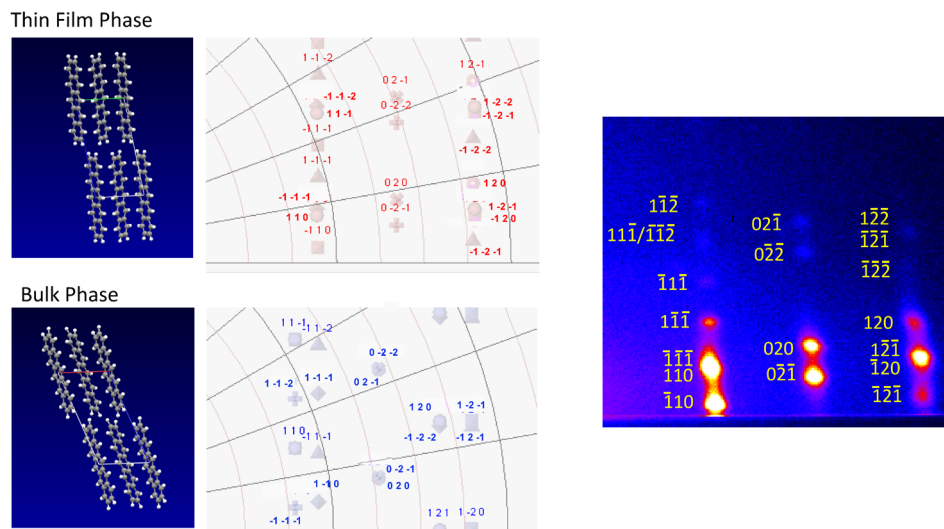


Fig. 8. Figures of molecular packing and results of reciprocal space simulation of pentacene of thin film phase (left up), and of bulk phase (left down) and the close-up view of GI-WAXS image marked in Fig. 7.

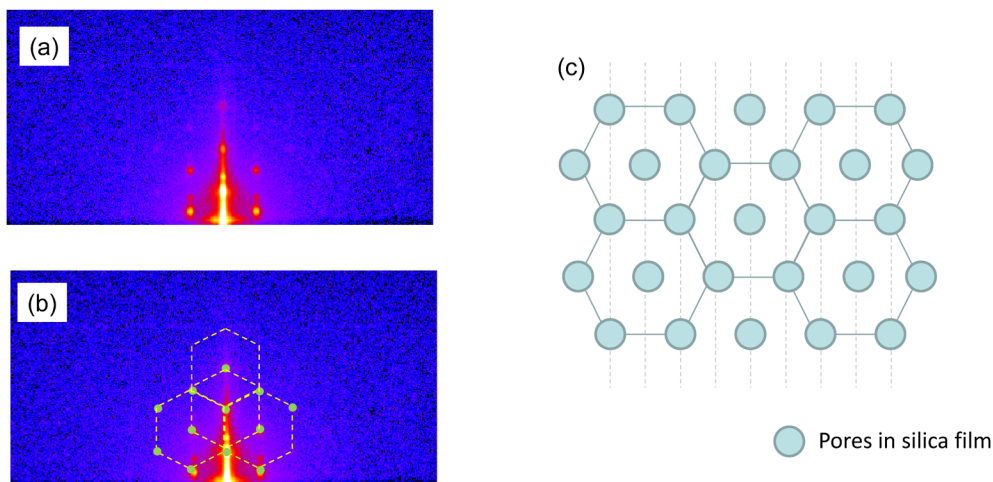


Fig. 9. (a) A diffraction image of GI-SAXS performed for mesoporous silica thin film. (b) A diffraction image with lattice pattern for the guide of eyes. (c) The extracted ideal ordering structure of pores in real space.

3.3. Long periodic structure analysis of mesoporous silica film

Diffraction signals from long periodic structured materials can be observed in the small angle region of scattering angles. In the analysis of these materials, it is not required for a 2D detector to cover a wide range of reciprocal space, since the region of interest is limited to the vicinity area of the direct X-ray beam. Instead, it is optimal for the detector to be positioned far away from the specimen to improve the angular resolution, by minimizing the apparent capture angles for each pixel of the detector. Figure 9(a) shows a diffraction image of GI-SAXS performed for structure analysis of mesoporous silica thin film deposited on a glass substrate. The incident angle of X-rays was set to 0.20° . In case of non-structured (random) arrangement of pores, a semicircle Debye–Scherrer ring should be observed,

but it is not true for the present case. The appearance of diffraction “spots” in this diffraction image indicates the existence of regular arrangements of pores in the silica film. By connecting diffraction spots, the hexagonal lattice pattern resulting from the regular arrangement of the pores was revealed (Fig. 8(b)), where an arrangement of pores with hexagonal closest packing in a certain cross-section may be suggested and the average interval of pores was calculated as 7.6 nm from this hexagonal lattice pattern. Further analysis is required, however, to understand the 3-dimensional arrangements of pores in this specimen, via similar approaches in studies by Miyata and Noma’s group^{(15)–(17)}.

4. Summary

Experimental approaches of 2D-WAXS and 2D-SAXS using a HyPix-3000 2D detector equipped

on SmartLab system were demonstrated, together with a latest 2D-SAXS/WAXS (reflection) attachment. This article, as Part 1, is focused on cases for polycrystalline thin films specimens with preferred orientation texture, where the approach for how to effectively collect weak signals from thin films is crucial for the analysis. For this purpose, grazing incident geometry was very important.

A forthcoming article, as Part 2, will be dedicated to cases analyzing epitaxial functional thin films with complex domain structures using a 2D detector.

References

- (1) S. Kobayashi and K. Inaba: *Rigaku Journal (English version)*, **28** (2012), No. 1, 8–13.
- (2) A. Ohbuchi: *Rigaku Journal (English version)*, **31** (2015), No. 1, 1–6.
- (3) Y. Shiramata: *Rigaku Journal (English version)*, **32** (2016), No. 2, 3–9.
- (4) K. Inaba, S. Kobayashi, K. Uehara, A. Okada, S.L. Reddy, and T. Endo: *Adv. Mater. Phys. Chem.*, **3** (2013), 72–89. (**Open Access**) <http://dx.doi.org/10.4236/ampc.2013.31A010>
- (5) T. Mitsunaga: *Rigaku Journal (English version)*, **25** (2009), No. 1, 7–12.
- (6) S. Kobayashi: *The Rigaku Journal (English version)*, **26** (2010), No. 1, 1–11.
- (7) T. Yamamoto, T. Yamada, A. Miyake, H. Makino and N. Yamamoto: *J. Soc. Inf. Display*, **16** (2008), No. 7, 713–719.
- (8) T. Yamada, H. Makino, N. Yamamoto and T. Yamamoto: *Jour. Appl. Phys.*, **107** (2010), 123534-1–123534-8.
- (9) J. Nomoto, H. Makino and T. Yamamoto: *Jour. Appl. Phys.*, **117** (2015), 045304-1–045304-9.
- (10) J. Nomoto, H. Makino and T. Yamamoto: *Thin Solid Films*, **601** (2016), 13–17.
- (11) J. Nomoto, H. Makino and T. Yamamoto: *Nanoscale Res. Lett.*, **11** (2016), 320-1–320-8. (**Open Access**) <http://nanoscalereslett.springeropen.com/articles/10.1186/s11671-016-1535-1>
- (12) J. Lee, J.H. Kim, S. Im and D.Y. Jung: *Jour. Appl. Phys.*, **96** (2007), 2301–2304.
- (13) T. Kakudate, N. Yoshimoto and Y. Saito: *Appl. Phys. Lett.*, **90** (2007), 081903-1–081903-3.
- (14) H. Yoshida, K. Inaba and N. Sato: *Appl. Phys. Lett.*, **90** (2007), 181930-1–181930-3.
- (15) T. Noma, H. Miyata, K. Takada and A. Iida: *Adv. X-ray Anal.*, **45** (2002), 359–364.
- (16) H. Miyata and K. Kuroda: *Chem. Mater.*, **12** (2000), 49–54.
- (17) H. Miyata and K. Kuroda: *Jour. Amer. Chem. Soc.*, **121** (1999), 7618–7624.